IEEE Access
Multidisciplinary | Rapid Review | Open Access Journal

Received September 5, 2019, accepted September 24, 2019, date of publication October 4, 2019, date of current version October 30, 2019.

Digital Object Identifier 10.1109/ACCESS.2019.2945635

High-Precision Calibration of Omnidirectional Camera Using an Iterative Method

XUANRUI GONG, YAOWEN LV, XIPING XU, ZHAOGUO JIANG, AND ZHUANG SUN

Key Laboratory of Opto-Electric Measurement and Optical Information Transmission Technology, Ministry of Education, School of Opto-Electronic Engineering, Changchun University of Science and Technology, Changchun 130033, China

Corresponding author: Yaowen Lv (lvyaowen2005@163.com)

This work was supported in part by the National Science Foundation (NSF) for Young Scientists of China under Grant 61803045 and Grant 61601195, in part by the Science and Technology Research Fund of Jilin Provincial Education Department under Grant JJKH20181134KJ, in part by the Science and Technology Innovation Fund of Changchun University of Science and Technology under Grant XJJLG-2017-05, and in part by the 111 Project of China under Grant D17017.

ABSTRACT A distorted checkerboard image affects the precision of omnidirectional camera calibration because of the inaccurate localization of the feature points. To solve this problem, an iterative refinement method is presented. First, the initial parameters are obtained using the traditional calibration method, and the distorted checkerboard is transformed to a distortion-free plane by the projection model that is estimated by initial parameters. Then, the feature point coordinates of the corrected image are extracted. The calibration parameters are recomputed using the refinement of new point locations until the camera parameters converge. This iterative refinement method improves the localization accuracy of feature points and, consequently, of camera calibration. The correctness and effectiveness of the method are verified by a series of simulations and physical experiments. The experiments show that the reprojection errors of feature points are reduced by 39% compared to traditional methods.

INDEX TERMS Omnidirectional camera calibration, feature point extraction.

I. INTRODUCTION

Since their introduction, omnidirectional cameras have been widely used in computer vision applications such as three-dimensional (3D) reconstruction, robot navigation [1], intelligent transportation, virtual reality and object localization. Camera calibration is a necessary step in extracting the measurement information from images. In previous studies, the omnidirectional calibration algorithms according to the calibration objects can be divided into line-calibration [2], [3], self-calibration [4], [5], two-dimensional (2D) planar pattern-based calibration [6]–[10], and 3D object pattern-based calibration [11], [12]. The accuracy of the image point locations has great significance for the camera calibration accuracy.

Classic feature point detection algorithms, such as Harris and Stephens [13] and Smith and Brady [14], have fast detection speeds. A feature point detector can realize the automatic detection of feature points. On this basis, later generations have made deeper studies to improve the feature detection accuracy. Wang and Wu [15] employed the Harris detector to first detect candidates and then remove the incorrect points by using the symmetry of the point coordinates and the interactions of the grid lines. Manoranjitham and Deepa [16] proposed the bilateral scale space construction calculation and used the Harris filter to detect extremes. Zheng *et al.* [17] used two convolutional templates and triangular part detectors that were combined to calculate point coordinates. Püspöki and Unser [18] proposed an improved filtering method to acquire exact coordinates. The algorithm has a faster calculation speed and better real-time performance. In those methods, the threshold is very important. However, it is often difficult to find a suitable threshold due to effects of noise, light and clutter.

In addition to feature detectors, some articles use geometric constraints to calculate feature point coordinates. Da Silva Tavares and Vaz [19] proposed the X angle was detected using the geometric features of the checkerboard pattern. Chu *et al.* [20] proposed image preprocessing was first performed using image dilation, and then the feature position was determined by detecting the circular template angle. He [21] calculated the subpixel using the constraint conditions between pixel values and coordinates. Those methods require orthogonal relationships between gradients and image

The associate editor coordinating the review of this manuscript and approving it for publication was Ruqiang Yan.

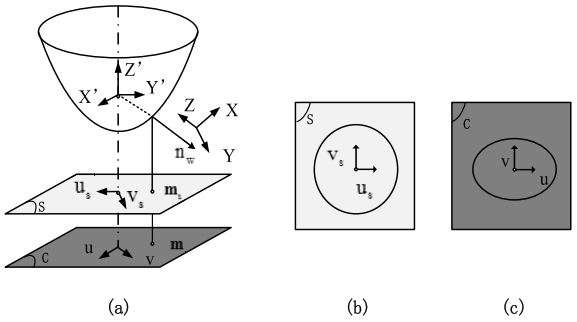

FIGURE 1. (a) Coordinate system. (b) Sensor plane. (c) Image plane.

edges, but this is not satisfied in the distorted omnidirectional images.

Determining how to improve the omnidirectional image feature point extraction precision to improve the calibration accuracy is the focus of this paper. Geiger *et al.* [23] first proposed the idea of locating the feature point coordinates in correcting images. Based on the characteristics of a panoramic camera and combined with this idea, we propose high-precision feature point extraction based on projection for omnidirectional camera calibration. First, we use the traditional calibration toolbox to calculate the camera parameters. Then, these parameters are used to estimate the projection model for projecting an image onto a distortion-free plane to obtain more precise feature point locations. The accurate feature points are then used to recalibrate the camera parameters. The previous process is repeated until the camera parameters converge. This paper calculates the initial parameters of the camera using the toolbox of [7]. Section 2 describes the model of the toolbox and the feature extraction algorithm, and Section 3 describes the principles in detail. The results of the simulation and physical experiments are shown in Sections 4 and 5 respectively. Finally, the paper is summarized in Section 6.

II. TRADITIONAL METHOD

A. CAMERA CALIBRATION MODEL

The omnidirectional camera model is a polynomial model that was defined by Scaramuzza *et al.* [7], as shown in Fig. 1. The scene point $\mathbf{n}_W = [X, Y, Z]^T$ is projected as an image point $\mathbf{m} = [u, v]^T$ that passes through the mirror to the sensor plane and then through the lens to the image plane. The relationship can be written as formula (1).

$$\lambda \cdot \mathbf{g}(\mathbf{m_s}) = \lambda \mathbf{g}(\mathbf{Am} + \mathbf{t}) = [\mathbf{R} \quad \mathbf{T}] \cdot \mathbf{n_w}, \quad \lambda > 0 \tag{1}$$

$$\mathbf{g}(u_s, v_s) = \begin{pmatrix} u_s \\ v_s \\ f(u_s, v_s) \end{pmatrix} = \begin{pmatrix} u_s \\ v_s \\ a_0 + a_1\rho \cdots a_n\rho^n \end{pmatrix} \tag{2}$$

$\mathbf{m_s} = [u_s, v_s]$ are the points on the sensor plane $\mathbf{S}$. The sensor plane is projected from the image plane through a rotation matrix $\mathbf{A} \in \Re^{2*2}$ and a translation matrix $\mathbf{t} \in \Re^{2*1}$. $\mathbf{g}$ is a nonlinear equation representing the camera imaging process, as shown in (2). f is the generic expression of the various forms of the mirror's construction. $\rho = \sqrt{u_s^2 + v_s^2}$ is the distance from the point to the center axis. The rotation matrix $\mathbf{R} \in \Re^{3*3}$ and translation vector $\mathbf{T} \in \Re^{3*1}$ are the camera motion parameters. λ is a constant indicating the depth scale.

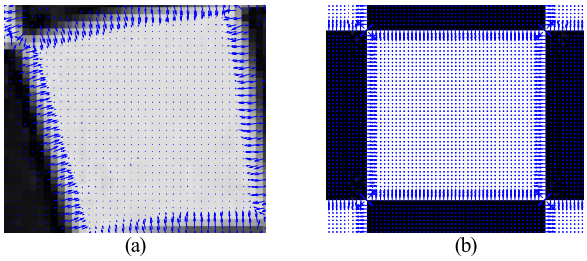

FIGURE 2. (a) Gradient of omnidirectional image. (b) Gradient of undistorted image.

An omnidirectional camera usually uses a hyperbolic or parabolic mirror, and so the first-order coefficient of function f is zero. The origin of the world coordinate system is on the calibration planar target, and so the Z value of point $\mathbf{n_w}$ on the calibration board is zero. $\mathbf{r_1}$, $\mathbf{r_2}$ and $\mathbf{r_3}$ are the column vectors in $\mathbf{R}$. By inserting (2) into (1), we can obtain a new function. We use $\mathbf{n_c} = [X', Y', Z']^T$ to represent the product of the last two matrices.

$$\lambda \begin{bmatrix} \mathbf{Am} + \mathbf{t} \\ a_0 + a_2\rho^2 \ldots a_n\rho^n \end{bmatrix} = \lambda \begin{bmatrix} u_s \\ v_s \\ a_0 + a_2\rho^2 \cdots a_n\rho \end{bmatrix} = \begin{bmatrix} \mathbf{r_1} & \mathbf{r_2} & \mathbf{T} \end{bmatrix} \begin{bmatrix} X \\ Y \\ 1 \end{bmatrix} \tag{3}$$

B. FEATURE EXTRACTION ALGORITHM

The traditional method performs the initial feature detection using the Harris interest point operator. Then, subpixel localization is used to further conduct a gradient-based search [23]. The orthogonal relationship between image coordinates and pixel gradients is written as (4)

$$\mathbf{q} = \arg\min_{\mathbf{q}'} \sum_{\mathbf{p} \in N_I(\mathbf{q}')} \left(\mathbf{Q}_\mathbf{p}^T * (\mathbf{p} - \mathbf{q}') \right)^2, \text{with } \mathbf{q}'^T * \mathbf{q}' = 1 \tag{4}$$

where $\mathbf{q}$ is a feature point location, $\mathbf{p}$ is the neighborhood coordinate in a local 11×11 pixel neighborhood N_I, and $\mathbf{Q_p}$ is the pixel gradient of $\mathbf{p}$. The subpixel coordinates of the feature points are calculated by setting the derivative of its Lagrangian to zero.

$$\mathbf{q} = \left(\sum_{\mathbf{p} \in N_I} \mathbf{Q_p} \mathbf{Q_p}^T \right) \sum_{\mathbf{p} \in N_I} \left(\mathbf{Q_p} \mathbf{Q_p}^T \right) * \mathbf{p} \tag{5}$$

In Fig. 2, it can be observed that the calibration pattern in the input images is distorted and that the pixel gradient is not perpendicular to the boundary, contradicting the assumption that was made. Therefore, subpixel coordinates cannot be calculated in this way. Fig. 2(b) shows the corrected distortion-free plane image. The corrected image can be used

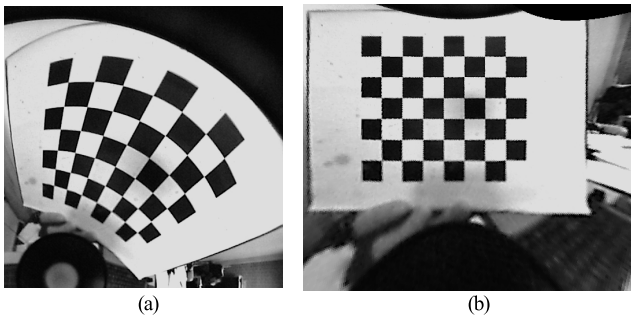

(a) (b)

FIGURE 3. (a) Omnidirectional camera distorted image. (b) Projection transformation image.

to more accurately extract the coordinates of the feature points because the image pixel gradient is perpendicular to the boundary.

III. ITERATIVE REFINEMENT METHOD

We use the calibration toolbox [7] that was given by Davide Scaramuzza to estimate the initial values of the camera. The calculation parameters that are required for calibration are $a_0 a_2 \cdots a_n$, the rotation matrix $\mathbf{R}$, the translation matrix $\mathbf{T}$, the distortion $\mathbf{A}$ and $\mathbf{t}$. Then, the camera parameters are used to calculate of the projection model. Using algebraic manipulation, (4) is rewritten as (6) to solve the point according to the known image point $\mathbf{m}$. $\mathbf{m}$ and $\mathbf{n_w}$ are the corresponding points in the image and in the world coordinate system, respectively. Then, the projection model is applied to project the points in the image to the world coordinate system. The x-o-y plane of the world coordinate system is selected as the image plane, and pixel values are assigned to the corresponding points. This completes the projection of the image to obtain a distortion-free image. Figs. 3(a) and (b) show the distorted image and corrected image, respectively.

$$\begin{bmatrix} X \\ Y \\ 1 \end{bmatrix} = \lambda [\, \mathbf{r}_1 \;\; \mathbf{r}_2 \;\; \mathbf{T} \,]^{-1} \begin{bmatrix} \mathbf{Am} + \mathbf{t} \\ a_0 + a_2\rho^2 \ldots a_n\rho^{\mathrm{n}} \end{bmatrix} \tag{6}$$

The feature coordinate of the distortion-free image is extracted using the method of Section 2. The coordinates of the points in the corrected image are converted to the coordinates of the corresponding points in the original image by reprojection.

$$\mathbf{g^{-1}}\,(\mathbf{n_c}) = \begin{pmatrix} \frac{X'}{\sqrt{X'^2+Y'^2}} \cdot \rho' \\ \frac{Y'}{\sqrt{X'^2+Y'^2}} \cdot \rho' \end{pmatrix} \tag{7}$$

$$a_0 + \frac{-Z'}{\sqrt{X'^2+Y'^2}}\rho' + a_2\rho'^2 + a_3\rho'^3 \cdots a_n\rho'^n = 0 \tag{8}$$

First, the feature point coordinate (X, Y) in the undistorted image is written as the homogeneous coordinate $(X, Y, 1)$. It is multiplied by the matrix $[\,\mathbf{r_1}\;\mathbf{r_2}\;\mathbf{T}\,]$ to obtain (X', Y', Z'). Then, solving (8), we substitute the maximum real root of ρ' into (7) and obtain $\mathbf{g^{-1}}\,(\mathbf{n_c})$. Finally, considering lens distortion, we use (9) to acquire the corresponding coordinate

Algorithm

1. **Detect feature points coordinate:** Detect checkerboard feature points' coordinate.
2. **Parameter Fitting:** Use the detected feature points to estimate camera parameters using calibration toolbox [7] .
3. **Project:** Use the camera parameters to project input image to distortion free plane.
4. **Localize feature points:** Using image coordinates and the pixel gradient, localize the points' sub-coordinates in the distortion-free plane.
5. **Reproject:** Project as the distorted image feature points coordinate using the camera parameters.
6. **Parameter Fitting :** Use the detected feature points to estimate camera parameters using calibration toolbox [7] .
7. **Iteration:** Repeat step 3 to step 6 until the parameters converge.

FIGURE 4. Camera calibration using the iterative refinement of feature points.

$\mathbf{m}$ in the original image.

$$\mathbf{m} = \left[\mathbf{A}^{-1} \cdot \mathbf{g}^{-1}\,(\mathbf{n_c})\right] - \mathbf{t} \tag{9}$$

New feature point coordinates are utilized to recalibrate the camera parameters. The updated camera parameters are used for a new round of calculations. Finally, we repeat the previous steps until the parameters converge. Fig. 4 shows the process of refining the camera parameters. We can calculate and refine the model parameters by applying the following steps.

IV. SIMULATION EXPERIMENT

A. FEATURE POINT COORDINATE ERROR ANALYSIS

In the proposed method, projection and reprojection are a pair of reciprocal processes. Due to the pixel dispersion, the reprojection of the corrected image is different from the original image. The performance of the projected transformation is explored to evaluate the subpixel location accuracy in this experiment. We set up an algebraic model that is analog camera imaging. The model is used to calculate the true position of feature points and generate simulated pictures. The feature point coordinates are extracted from the simulated image by the proposed method and traditional method and compared with the real position. The internal parameters of the algebraic model are as follows: $a_0 = 206.16$, $a_2 = 0.00451$, $x_c = 977$, $y_c = 531$, A=(1,0;0,1) and t=(0,0). The feature points of the planar object used to generate the simulated picture are 6×7, and the square is 30 mm. We performed 50 experiments with randomly generated motion parameters. The constraint is the norm of the translation vector equal to 400. The experimental

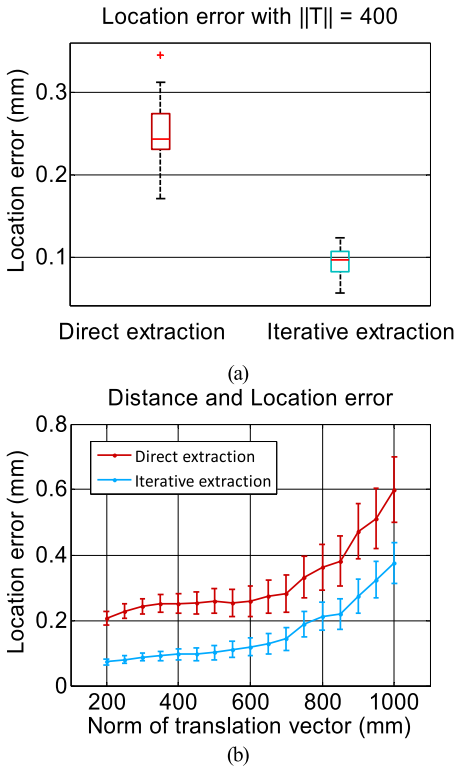

FIGURE 5. (a) Location error with ||T|| = 400. (b) Norms of the translation vector and location errors.

results are shown in Fig. 5(a). The thin horizontal red line in the blue rectangle or red rectangle represents the mean value of the location error. The rectangle shows 50% of the location error distributes in the vicinity of the mean value. It is obvious that the rectangle in the iterative method is smaller than that of direct extraction, which means the distribution of the location error in the iterative method is more concentrated.

Then, the relationship between the coordinate error and the distance from the checkerboard to the camera is explored by keeping the rotation matrix unchanged and changing the norm of the translation vector. Fig. 5(b) shows the variations of the errors of the feature point coordinates that are extracted using different methods. As the distance from the checkerboard to the camera increases, the pixels that are occupied by the checkerboard on the picture decrease. Therefore, the accuracy of the feature point coordinates is reduced. When the norm of the translation vector is 850 mm, the iteration extraction and direct extraction errors are, respectively, 0.2 and 0.43. The iteration extraction method improves the feature point location accuracy and increases the applicable distance of the calibration plate. To ensure the positioning accuracy of the feature point coordinates, when shooting the calibration image, the checkerboard should be guaranteed to be within 900 mm.

B. THE REPROJECTION ERRORS IN SIMULATION IMAGES

Simulation experiments can compare the calibration values with the ground truth values and explore the effects of noise on the traditional methods and proposed methods. The image

TABLE 1. Camera parameters and errors.

parameter		original value	traditional algorithm	our algorithm
a_0	value	131.91	131.36	131.68
	Error%	0	0.417	0.175
a_1	value	0.0019	0.00019	0.0019
	Error%	0	0.736	0.526
x_c	value	392.38	391.91	392.5
	Error%	0	0.121	0.031
y_c	value	514.57	514.25	514.55
	Error%	0	0.0965	0.0384
c	value	0.9988	1.0011	1.0007
	Error%	0	0.23	0.19

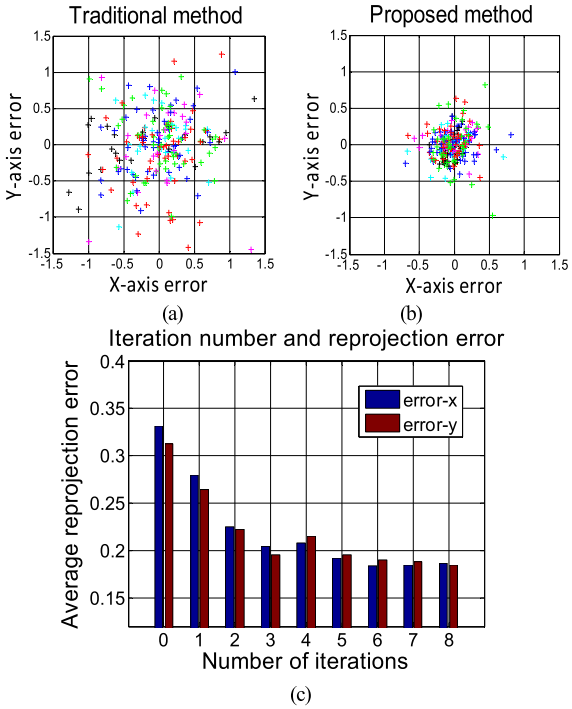

FIGURE 6. Reprojection errors of the target feature points. (a) Traditional method, (b) proposed method, and (c) reprojection errors with respect to the number of Iterations.

resolution is 1024×768 pixels, and the planar target with 6×7 feature points is used for the calibration. The mirror function is a 2nd-order polynomial. Matrix A is expressed as A = (c, 0; 0; 1) and t = (0, 0). Other parameters are shown in the first row of TABLE 1. The outer parameter matrix is randomly generated, and the mode length of the translation matrix is between 300 and 500 mm. The simulated images are used to perform 8 iterations. Each iteration average reprojection error is shown in Fig. 6.

Figs. 6(a) and (b) show the reprojection errors of the feature points based on the proposed method and traditional method, respectively. The average reprojection error of the proposed method is 0.27 pixels, while that of the traditional method is 0.44 pixels. The average reprojection error is reduced by 38.6%. Fig. 6(c) is the statistical histogram of the average reprojection error for each iteration. As can be seen, the average reprojection error is gradually reduced and the numerical solutions converge after three or four iterations; therefore,

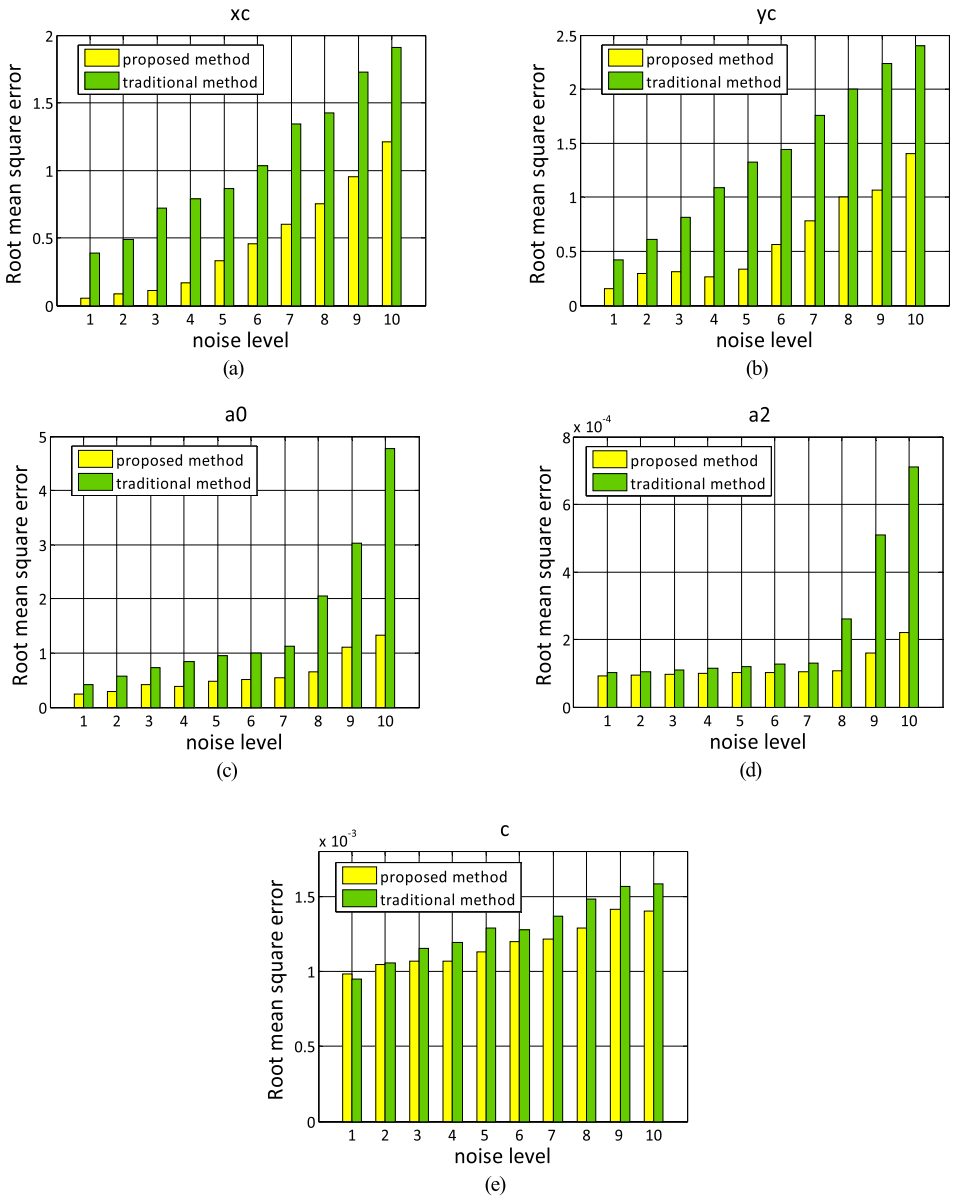

FIGURE 7. Parameter root mean square error (a) the error of xc, (b) the error of yc, (c) the error of the zero-order mirror parameters a0, (d) the error of the second-order specular parameter a2, and (e) the error of the distortion coefficient c.

four iterations are recommended in the proposed methods. In addition, we evaluate the performances of the calibration method by comparing the errors of the calibration results with the ground truth value, and the results are shown in TABLE 1. It is shown that parameters' errors based on the proposed method are smaller than those of the traditional method.

C. ROOT MEAN SQUARE ERROR (RMSE) OF THE CAMERA PARAMETERS

Then, Gaussian noise is added to the pixels of the simulation image to assess their impact on the calibration accuracy. The mean of the Gaussian noise is zero, and the maximum variance is 38.25. The variance is divided into 10 orders of magnitude. For each level, 100 experiments are set up based on the traditional method and the proposed method, and four iterations are executed.

Figs. 7(a) and (b) show that the center coordinate errors of the traditional method are twice those of the proposed method. For the mirror's parameter errors, the errors of the traditional method are two to three times those of the proposed method. The image distortion errors of the two methods, as shown in Fig. 7(e), are similar.

V. PHYSICAL EXPERIMENT

A. THE REPROJECTION ERRORS IN CALIBRATION TOOLBOX IMAGES

First, an experiment with the standard images is conducted using the camera calibration toolbox [24]. The image was

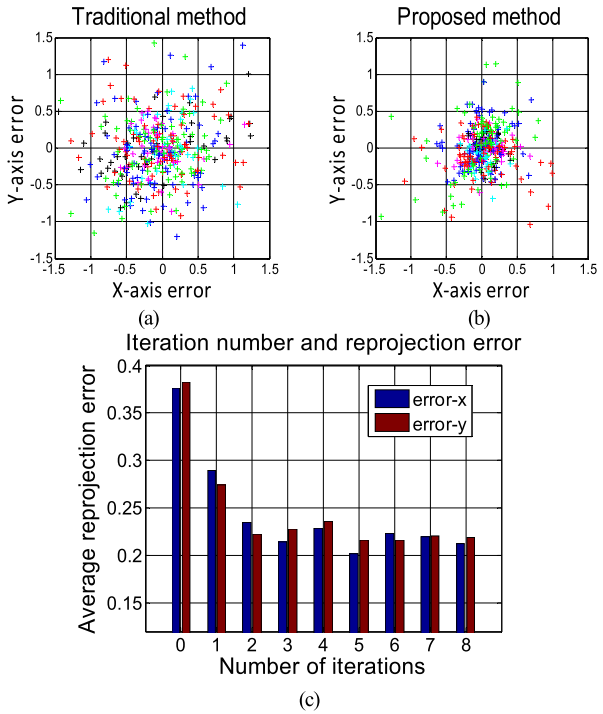

FIGURE 8. Reprojection errors of the target feature points: (a) the traditional method, (b) the proposed method, and (c) reprojection errors with respect to the number of Iterations.

FIGURE 9. The physical experiment's omnidirectional camera.

taken using a catadioptric omnidirectional system, which consists of a hyperbolic mirror and a normal camera with 1024×768 pixels. The method that is described herein and traditional methods are performed. The calibration reprojection errors of the feature points based on the traditional method and proposed method are shown in Figs. 8(a) and (b), respectively. The reprojection errors of the proposed method, which are reduced from 0.52 pixels to 0.31 pixels, are 0.6 of those using the traditional method. Fig. 8(c) shows the average reprojection errors as the number of iterations increases.

B. THE REPROJECTION ERRORS IN REAL IMAGES

In this experiment, an omnidirectional camera that is shown in Fig. 9 is used. The image resolution is 768×1024 pixels.

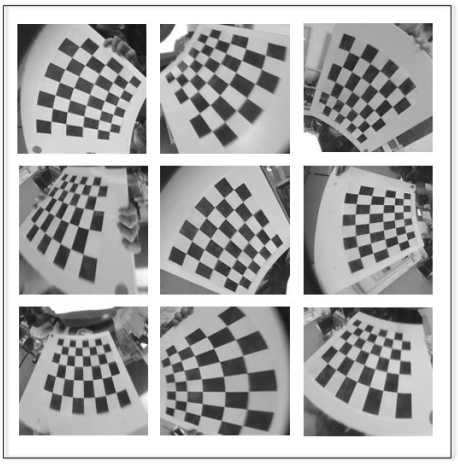

FIGURE 10. Images that are used for calibration.

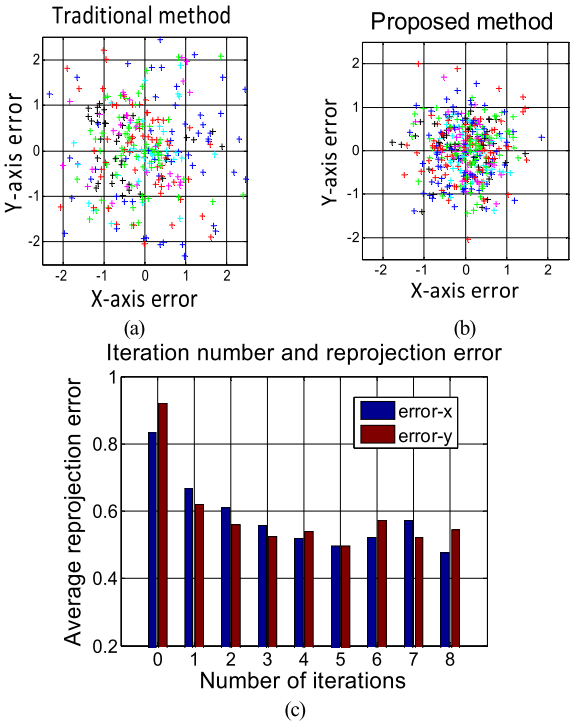

FIGURE 11. Reprojection errors of the target feature points: (a) the traditional method, (b) the proposed method, and (c) reprojection errors with respect to the number of iterations.

There are 5×6 feature points on the planar target. The calibration images are shown in Fig. 10.

Fig. 11 shows the experimental results. Figs. 11(a) and (b) are the calibration reprojection errors of the traditional method and proposed method, respectively. The average reprojection errors in the X and Y directions as the number of iterations increases are shown in Fig. 11 (c). After three iterations, the reprojection errors are asymptotically stable. The experiments prove that the proposed method universally improves the calibration accuracy. Regardless of whether it

TABLE 2. Feature point extraction time.

Time	Simulation images	Toolbox images	Real images
Direct extraction	0.65 s	0.82 s	1.12 s
The proposed method	1.09 s	1.28 s	1.56 s

assesses the sample images in the calibration toolbox or the images that are taken by the camera, the calibration accuracy is improved by approximately 39%.

C. THE REPROJECTION ERRORS IN REAL IMAGES

We used MATLAB 2014a to test the time of feature point extraction for 3 different images. The test computer is an Intel(R) Core(TM) i5-4460 3.20 Hz CPU and a 64-bit operating system. The average time costs of one image are shown in Table (2). Table (2) shows that the real image takes more time for feature point extraction than the simulated image. The main reason is that the contrast of the simulated image is strong and the point features protrude. High contrast can improve the feature point extraction speed. In addition, due to image correction and corner relocation, the proposed method is more time-consuming. However, the accuracy of the vision measurement system is influenced by the calibration accuracy. Once the camera is calibrated, the parameters are constant. Therefore, the calibration accuracy is more important than the computing time. The improved precision is worth the higher computational costs.

VI. CONCLUSION

In this paper, we propose a method for accurate omnidirectional camera calibration using checkerboard pattern images. To decrease the feature point extraction error, a projection model is proposed that converts the checkerboard pattern to a distortion-free plane. Then, the feature point coordinates are extracted on the undistorted plane and applied to determine the original image coordinates using the reprojection model. According to the new feature coordinates, the camera parameters are iteratively calculated until they converge. A series of simulations and physical experiments were designed to verify the performance of the proposed method. Comparing the results of physical experiments, our method improves the different mirror and different camera parameters' calibration results by reducing the reprojection errors of the target feature points by 39%. The results of the simulation experiments show that when the noise increases, the RMSE of each parameter of the camera is half that of the conventional method. We also compare the camera calibration limit distance in the traditional methods and proposed methods. In addition, the proposed method is independent of the calibration model. Our method can be combined with all kinds of omnidirectional camera calibration toolboxes to make the calibration results more precise. In future works, different calibration objects and models will be developed.

ACKNOWLEDGMENT

The authors would like to thank the National Demonstration Center for Experimental Opto-Electronic Engineering Education for the use of their equipment.

REFERENCES

[1] M. Liu, C. Pradalier, and R. Siegwart, "Visual homing from scale with an uncalibrated omnidirectional camera," *IEEE Trans. Robot.*, vol. 29, no. 6, pp. 1353–1365, Dec. 2013.

[2] Y. Zhao, Y. Li, and B. Zheng, "Calibrating a paracatadioptric camera by the property of the polar of a point at infinity with respect to a circle," *Appl. Opt.*, vol. 57, no. 15, pp. 4345–4352, May 2018.

[3] F. Wu, F. Duan, Y. Wu, and Z. Hu, "A new linear algorithm for calibrating central catadioptric cameras," *Pattern Recognit.*, vol. 41, no. 10, pp. 3166–3172, Oct. 2008.

[4] Y. Zhao and Y. Li, "Camera self-calibration from projection silhouettes of an object in double planar mirrors," *J. Opt. Soc. Amer. A*, vol. 34, no. 5, pp. 695–707, 2017.

[5] X. Deng, F. Wu, Y. Wu, F. Duan, L. Chang, and H. Wang, "Self-calibration of hybrid central catadioptric and perspective cameras," *Comput. Vis. Image Understand.*, vol. 116, no. 6, pp. 715–729, Feb. 2012.

[6] Y. Zhao and Y. Wang, "Intrinsic parameter determination of a paracatadioptric camera by the intersection of two sphere projections," *J. Opt. Soc. Amer. A.*, vol. 32, pp. 2201–2209, Nov. 2015.

[7] D. Scaramuzza, A. Martinelli, and R. Siegwart, "A toolbox for easily calibrating omnidirectional cameras," in *Proc. IEEE IROS*, Beijing, China, Oct. 2006, pp. 5695–5701.

[8] C. Mei and P. Rives, "Single view point omnidirectional camera calibration from planar grids," in *Proc. IEEE ICRA*, Roma, Italy, Apr. 2007, pp. 3945–3950.

[9] H. Duan and Y. Wu, "A calibration method for paracatadioptric camera from sphere images," *Pattern Recognit. Lett.*, vol. 33, no. 6, pp. 677–684, Dec. 2012.

[10] Y. Li and Y. Zhao, "Calibration of a paracatadioptric camera by projection imaging of a single sphere," *Appl. Opt.*, vol. 56, no. 8, pp. 2230–2240, Mar. 2017.

[11] L. Puig, Y. Bastanlar, P. Sturm, J. J. Guerrero, and J. Barreto, "Calibration of central catadioptric cameras using a DLT-like approach," *Int. J. Comput. Vis.*, vol. 93, no. 1, pp. 101–114, Dec. 2011.

[12] Y. Wu and Z. Hu, "Geometric invariants and applications under catadioptric camera model," in *Proc. IEEE ICCV*, Beijing, China, Oct. 2005 pp. 1547–1554.

[13] C. G. Harris and M. Stephens, "A combined corner and edge detector," in *Proc. Alvey Vis. Conf.*, vol. 15, Aug. 1988, pp. 147–151.

[14] S. M. Smith and J. M. Brady, "SUSAN—A new approach to low level image processing," *Int. J. Comput. Vis.*, vol. 23, no. 1, pp. 45–78, 1997.

[15] Z. Wang, X. Xu, D. Xue, and W. Wu, "Recognition and location of the internal corners of planar checkerboard calibration pattern image," *Appl. Math. Comput.*, vol. 185, no. 2, pp. 894–906, Feb. 2007.

[16] R. Manoranjitham and P. Deepa, "Novel interest point detector using bilateral-Harris corner method," in *Proc. ICACCS*, Coimbatore, India, Jan. 2017, pp. 1–4.

[17] Z. Zheng, Z. Zha, L. Han, and Z. Wang, "Feature detection and correspondence for camera calibration," *Int. J. Inf. Acquisition*, vol. 5, no. 1, pp. 41–50, Jan. 2008.

[18] Z. Püspöki and M. Unser, "Template-free wavelet-based detection of local symmetries," *IEEE Trans. Image Process.*, vol. 24, no. 10, pp. 3009–3018, Oct. 2015.

[19] P. Da S. Tavares and M. A. P. Vaz, "Accurate subpixel corner detection on planar camera calibration targets," *Opt. Eng.*, vol. 46, no. 10, Oct. 2007, Art. no. 107205.

[20] J. Chu, A. Guolu, and L. Wang, "Chessboard corner detection under image physical coordinate," *Opt. Laser Technol.*, vol. 48, pp. 599–605, Jun. 2013.

[21] H. He and S. Huang, "Improved algorithm for Harris rapid sub-pixel corners detection," *J. Image Graph.*, vol. 17, no. 7, pp. 853–857, 2012.

[22] A. Datta, J.-S. Kim, and T. Kanade, "Accurate camera calibration using iterative refinement of control points," in *Proc. IEEE ICCV Workshops*, Sep./Oct. 2009, pp. 1201–1208.

[23] A. Geiger, F. Moosmann, Ö. Car, and B. Schuster, "Automatic camera and range sensor calibration using a single shot," in *Proc. IEEE Int. Conf. Robot. Automat. (ICRA)*, Saint Paul, MN, USA, May 2012, pp. 3936–3943.
[24] [Online]. Available: https://sites.google.com/site/scarabotix/ocamcalib-toolbox

XUANRUI GONG received the B.S. degree in photoelectric information science and engineering from Henan Normal University, China, in 2017. She is currently pursuing the Ph.D. degree with the Changchun University of Science and Technology. Her research interests include the target recognition and tracking of the based on catadioptric camera.

YAOWEN LV received the Ph.D. degree from the Graduate School of Chinese Academy of Sciences, in 2014. He is currently an Assistant Professor with the School of Optoelectronic Engineering, Changchun University of Science and Technology. His research interests include computer vision and pattern recognition.

XIPING XU received the B.S. degree from the Electronic Engineering of Changchun Optics Precision Mechanical School, China, in 1993, the M.S. degree, in 1999, and the Ph.D. degree from the Changchun University of Science and Technology, China, in 2004, where he is currently a Professor and a Doctoral Supervisor with the College of Optoelectronic Engineering. His research interests include image processing, signal processing, photoelectric detection technology, and modern photoelectric sensing technology.

ZHAOGUO JIANG received the Ph.D. degree from the University of California at Berkeley, in 1995. In 2006, he returned to China and founded Polar Multimedia Technology (Shanghai) Company Ltd., serving as the Chairman and the President. His research interests include optical measurement and optical instrument design.

ZHUANG SUN received the bachelor's degree from the Changchun University of Science and Technology, in 2017, where he is currently pursuing the master's degree. His research interest includes 3D reconstruction.